

13th CIRP Conference on Photonic Technologies [LANE 2024], 15-19 September 2024, Fürth, Germany

# Improvement of manufacturing accuracy of graded Ti-6Al-4V BCC lattice structures by local laser power adaption

Nico Ulff<sup>\*,a</sup>, Eric Leingang<sup>a</sup>, Johannes Schubert<sup>a</sup>, Frederik Zanger<sup>a</sup>

<sup>a</sup> Institute of Production Science (wbk), Karlsruhe Institute of Technology (KIT), Kaiserstraße 12, 76131 Karlsruhe, Germany

\* Corresponding author. Tel.: +49-721-608-44288; E-mail address: [nico.ulff@kit.edu](mailto:nico.ulff@kit.edu)

## Abstract

Additive Manufacturing by laser powder bed fusion (PBF-LB/M) enables the manufacturing of metallic implants with graded lattice structures, adapting the porosity and stiffness of the implant with cortical and trabecular bone for improved osseointegration. One drawback is the manufacturing accuracy of graded lattice structures due to deviating process strategies. Minimal structures with diameters < 150 µm require low energy input to avoid overmelting. Conversely, larger structures (> 200 µm) are then prone to insufficient melting and require higher energy input. This prevents a combination into one graded structure using standard strategies, which can result in deviations of up to 50%. Investigations show that adjusting the energy input at down-skin surfaces enables a more precise manufacturing for graded BCC lattice structures (ranging from 100 – 300 µm) without severe compromise for one size region. Furthermore, this approach also reduces the deviation for specific structure sizes to less than 2%.

© 2024 The Authors. Published by Elsevier B.V.

This is an open access article under the CC BY-NC-ND license (<https://creativecommons.org/licenses/by-nc-nd/4.0>)

Peer-review under responsibility of the international review committee of the 13th CIRP Conference on Photonic Technologies [LANE 2024]

**Keywords:** Powder Bed Fusion, graded lattice structure, down-skin, Ti-6Al-4V

## 1. Introduction

Additive Manufacturing (AM) especially laser powder bed fusion (PBF-LB/M) enables the manufacturing of advanced and customized implants with increased biocompatibility compared to conventional manufacturing methods [1]. Due to a mismatch in mechanical strength compared to natural bone (Young's modulus of trabecular bone = 1-5 GPa, ranging from 100 – 200 µm feature thickness) and biocompatible materials such as Ti-6Al-4V grade 23 for implants (~ 110 GPa), stress shielding would occur, leading to bone atrophy [2-4].

AM enables the manufacturing of bone like lattice structures, which can be altered in regard to the desired stiffness and porosity of the implant for mimicking trabecular or cortical bone for better osseointegration [5]. This requires fine structure sizes (100 – 300 µm), specific volume fractions (70-90%) and pore sizes for cell attachment and adequate ingrowth (300 – 900 µm) [6,7]. Implementing graded or altered structures

further improve the stiffness-matching [8,9]. This leads to process related challenges and advanced process strategies for minimal structure sizes compared to bulk solid components with possible strategies such as the common used contour-hatch strategy, single contour scanning or single exposure strategies [10-12]. Instead of the widely used volumetric energy density (VED) or line energy density (LED), dimensionless scaling laws including a more thermodynamic approach including enthalpy laws can be used for process window development of bulk solid parts [13] or strut diameter scaling of lattice structures [14] and are applicable for estimating melt pool characteristics [15].

Since the target structure sizes are at the limit of manufacturability on standard PBF-LB systems, the resulting strut geometry is highly dependent on the melt pool geometry, which can lead to typical geometric deviations in micro-lattice structures shown in Figure 1 [14,16,17]:

- necking
- overmelting (elliptical and deformed struts)
- waviness

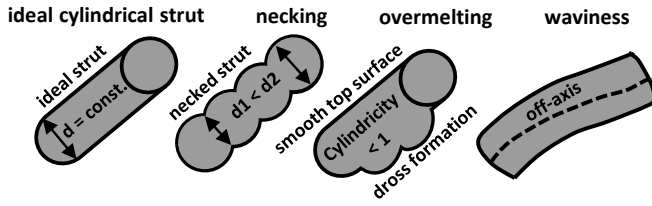


Fig. 1. Typical geometric deviations in micro-lattice structures (necking, overmelting, waviness)

Since geometric deviations can reduce mechanical strength by up to 50% compared to the predicted nominal Young's modulus, strategies for improvement must be addressed [16].

Additionally, the layer-by-layer process sequence and the stair stepping effect result in angle dependent oversizing for inclined struts in comparison to a vertical orientation [14]. For example, 20° oriented struts have nearly double the size compared to vertical struts and their nominal diameter on average deviates up to 11.9% [18]. This can be explained by the fact that the amount of powder exposed by the laser increases with increasing inclination angle [19] and that the heat conduction through powder is much worse compared to solid structures, leading to heat accumulation and therefore a direction dependent oversizing [20,21].

This phenomenon has been widely described in literature [18,22], but strategies for overcoming this effect are limited, especially in the region of diameters < 300  $\mu\text{m}$ . For example, a design-oriented approach can improve accuracy [23], by predicting the angle dependent deviation and compensation in the initial geometry. In contrast, process-oriented adaptations offer a more extensive approach for several lattice types. On the one hand, a general beam-offset of the contour-scan leads to an improved manufacturing accuracy [24]. In addition, scan areas can be divided into top- and down-skin areas for further improvement. In [25] a novel scan-strategy was introduced, by first implementing a low amount of energy to the loose powder (down-skin area) with an offset and then scanning the solid sections (filling area) by re-melting several previous layers, also increasing manufacturing accuracy and enabling inclination angles down to 10° with tolerable strut quality for diameters > 500  $\mu\text{m}$ . A similar approach was shown in [26] by reducing the down-skin energy for cubic lattices (only vertical and horizontal struts) improving the manufacturing accuracy for horizontal struts with diameters > 700  $\mu\text{m}$ .

In this paper, a general applicability of down-skin parameter adjustments for a more accurate and simple manufacturing of micro-lattices for standard PBF-LB setups, conducted in [27], was further improved for Ti-6Al-4V. The best results were transferred to BCC lattice structures with nominal diameters of 100-300  $\mu\text{m}$ . Furthermore, a transfer of this approach is also applicable for graded micro-lattices without the necessity of deviating strategies or process parameters for minimal structure sizes and upscaling.

|                  |   |
|------------------|---|
| LED              | Line energy density in J/mm                     |
| LED <sub>T</sub> | Line energy density in top-skin region in J/mm  |
| LED <sub>D</sub> | Line energy density in down-skin region in J/mm |
| $\Theta$         | Inclination angle in °                          |
| $c_d$            | Contour distance in $\mu\text{m}$               |
| $h_d$            | Hatch distance in $\mu\text{m}$                 |

## 2. Experimental setup and methodology

### 2.1. PBF-LB process adjustment and sample production

All samples analyzed in this work were manufactured on a SLM 280 HL machine (SLM Solutions, Lübeck, Germany), equipped with a 400 W continuous wave laser by IPG with an 80  $\mu\text{m}$  spot diameter in argon atmosphere and a set layer thickness of 30  $\mu\text{m}$ . The employed raw powder by m4p material solutions GmbH (Ti-6Al-4V grade 23) with a particle size range D10-D90 of 15-45  $\mu\text{m}$  was used.

The experiments were carried out in three stages. In order to evaluate the struts with as few CT measurements as possible,

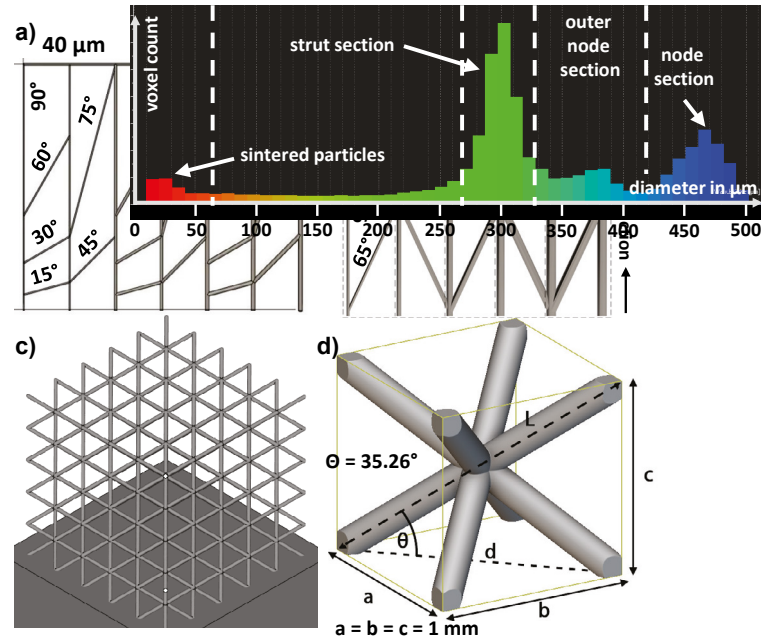


Fig. 2. (a) Test geometry for minimal structures and general influence of energy input; (b) Test geometry for down-skin process optimization; (c) Exemplary BCC lattice structure (100  $\mu\text{m}$ ); (d) Geometrical illustration BCC unit cell and specific inclination angle (35.26°)

for each stage a specific test geometry was designed, shown in Figure 2. First, a basic process window and manufacturing limit for micro-struts was established by conducting a full factorial DoE study, including the following parameters (laser power  $P = 30 \text{ W}, 50 \text{ W}, 70 \text{ W}$ ; scan velocity  $v = 200\text{-}1000 \text{ mm/s}$ ; contour distance  $c_d = 40\text{-}120 \text{ }\mu\text{m}$  and inclination angles ranging from 15°-90°) with three repetitions each. In addition to the strut diameters, the strut quality was qualitatively assessed in order to obtain a starting point for the local parameter adjustment. In order to also check for transferability to graded lattice structures, the test geometry was extended by the specific inclination angle of BCC structures (35.26°), the geometrical context is illustrated in Fig. 2 (d). An inclination

### Nomenclature

|     |  |
|-----|--|
| VED | Volumetric energy density in J/mm <sup>3</sup> |
|-----|--|

of  $75^\circ$  was excluded, as the direction-dependent influence for angles  $> 65^\circ$  was classified as negligible. The designed diameters were investigated in  $50\ \mu\text{m}$  steps ranging from  $100\ \mu\text{m}$  to  $300\ \mu\text{m}$ , showcased in Fig. 2 (b), with three repetitions each. In order to evaluate the influence of the local laser adjustment, the contour was exposed with deviating LED values, which represents the ratio of  $P$  to  $v$  in  $\text{J}/\text{mm}$ , and subdivided into a top-skin region ( $\text{LED}_T = \text{const.}$ ) and a down-skin area ( $\text{LED}_D < \text{LED}_T$ ), shown in Fig. 3 (a). The best results were transferred to BCC lattice structures of  $100\text{--}300\ \mu\text{m}$  with five unit cells of  $1\ \text{mm}$  in each direction, represented in Fig. 2 (c). In order to avoid increased lack of fusion defects, an internal hatching with a VED of  $65\ \text{J}/\text{mm}^3$  with the following parameters was used ( $P = 50\ \text{W}$ ,  $h_d = 52\ \mu\text{m}$ ,  $v = 493\ \text{mm}/\text{s}$ ) in regard to [28].

## 2.2. Geometry and density evaluation

The test specimens were scanned in a Metrotom 800 CT device by Zeiss IMT GmbH (Germany). Samples were scanned

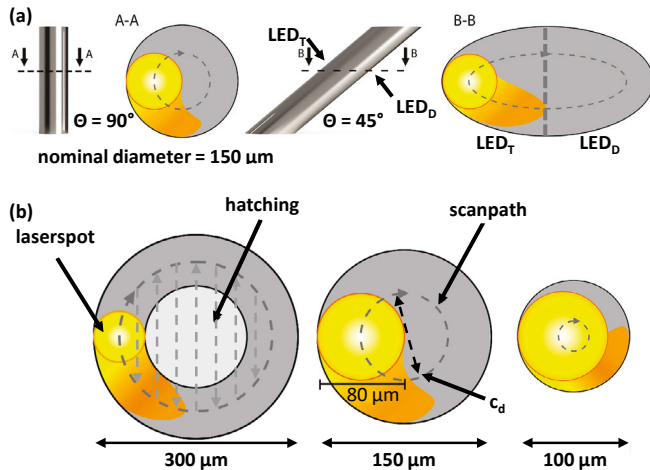


Fig.3. Geometric correlation of the process parameters with the inclination angle (a) and the nominal diameter of struts (b).

in a single  $360^\circ$  scan without stitching; the source voltage and current were set to  $130\ \text{kV}$  and  $30\ \mu\text{A}$ . A  $0.25\ \text{mm}$  Cu beam hardening filter was used to improve the image contrast (resulting voxel size =  $5\ \mu\text{m}$ ). The reconstruction was calculated on the CT device using its software Metrotom OS 3.2 by Zeiss IMT GmbH (Germany). VGStudioMax 3.4 by VGStudio (Germany) was used for analyzing the internal porosity (VGEasyPore algorithm) and resulting strut diameter (thickness measurement with sphere method). This method was used to determine the maximum inscribed circle of singular struts and lattice structures. Fig. 4 shows that a BCC structure, for example, can be distinguished in specific regions (sintered particles on the surface, a strut section without adherent particles and a node section). Since implant structures are usually post-processed in order to reduce the surface roughness and specifically remove sintered particles [29], the maximum inscribed circle was chosen as measured strut diameter value.

Fig. 4. Exemplary histogram of a BCC structure ( $300\ \mu\text{m}$  nominal diameter) and corresponding specific regions.

## 3. Results and discussion

### 3.1. General influence of energy input

To evaluate the fundamental influence of  $c_d$ ,  $P$  and  $v$  on the quality of micro-struts as a function of inclination angle, the geometric characteristics and strut diameters were assessed qualitatively in Fig. 5 in accordance to Fig. 1. A sharp decrease in quality can be seen for inclination angles  $< 60^\circ$ , with the struts tending to either overmelt if the energy input is too high, or to neck and even fail to build up if the energy input is too low, resulting in an undesirable quality, with examples manufactured as shown in Fig. 6.

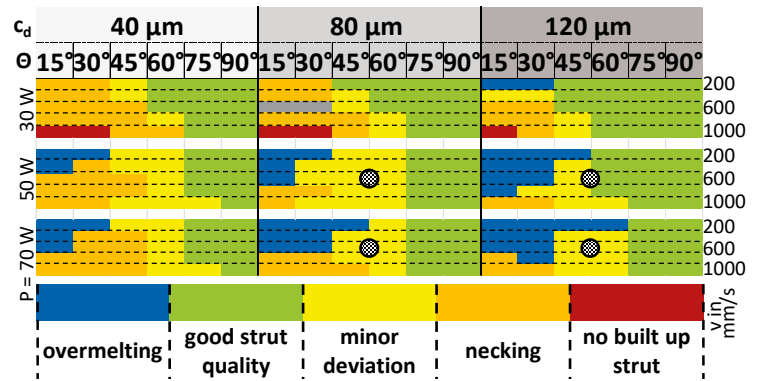


Fig. 5. Qualitative assessment on influence of energy input on geometry characteristics and resulting strut diameter in  $\mu\text{m}$

The manufactured diameters in stage one ranged from  $103\text{--}245\ \mu\text{m}$  and two sets of  $\text{LED}_T$  with  $0.083\ \text{J}/\text{mm}$  and  $0.125\ \text{J}/\text{mm}$  were chosen for stage two (region of further adjustment is indicated in Fig. 5.), as lower inclination angles mainly tended to overmelt, while manufactured struts with diameters  $> 60^\circ$  were in range to the desired nominal diameter.

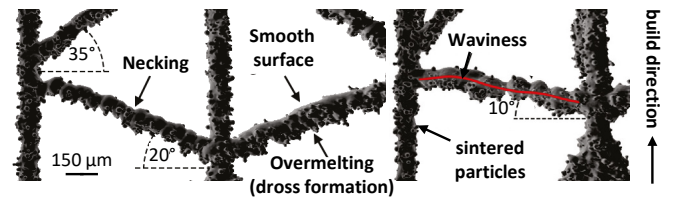


Fig. 6. Exemplary geometrical defects of manufactured micro-struts



### 3.2. Down-Skin process optimization

After a general assessment, different sets of  $LED_D$  were applied to the test geometry of Fig. 2 (b) with the following values (0.03; 0.038; 0.05; 0.067; 0.083 J/mm and  $LED_T = LED_D$ ). Fig. 7. shows the analytical depiction of the exposed powder surface area depending on nominal strut diameter and inclination angle, indicating that smaller diameters are more prone to overmelting and oversizing.

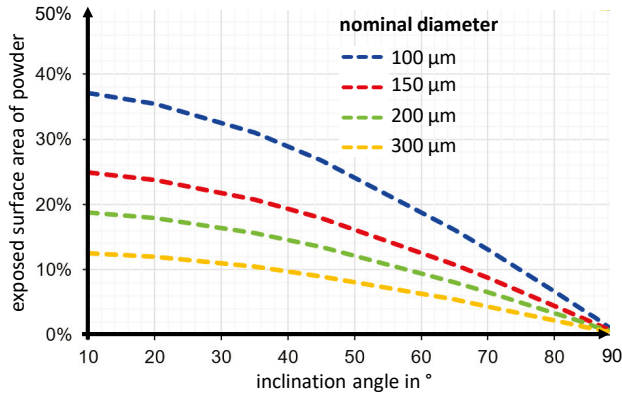


Fig. 7. Analytical depiction of the exposed powder surface area depending on nominal strut diameter and inclination angle

The assumption could be confirmed with the results shown in Figure 8, using the example of an inclination angle of 20° for  $LED_T = 0.125$  J/mm, demonstrating an almost linear relationship with increasing  $LED_D$  and the resulting deviation.

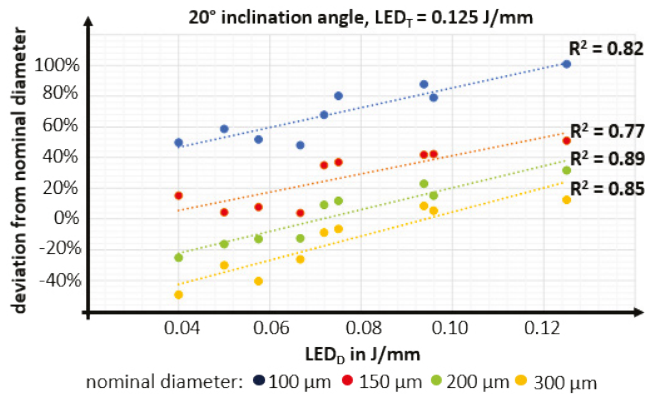


Fig. 8. Influence of  $LED_D$  on the resulting deviation from the nominal diameter

Although individual combinations were in the range of almost 0% deviation, a slightly too high  $LED_T$  value led to a strong oversizing for a nominal diameter of 100 μm, whereas a too low  $LED_D$  value even fell short of the nominal dimension by up to 40%. This can be explained by the fact that a too low  $LED_D$  value is not sufficient and only increases the number of sintered particles instead of generating a stable melt pool.

In contrast, Figure 9 shows the influence of the lower  $LED_D$  on the resulting diameter as a function of the inclination angle for nominal diameters of 100–200 μm, compared to no local adjustment (full lines). The standard deviations were not specified for the purpose of visualization.

The specific angle of 35°, marked with a dashed vertical line, is of significant importance for the transfer to BCC lattice structures. On the one hand, it was possible to produce a high-

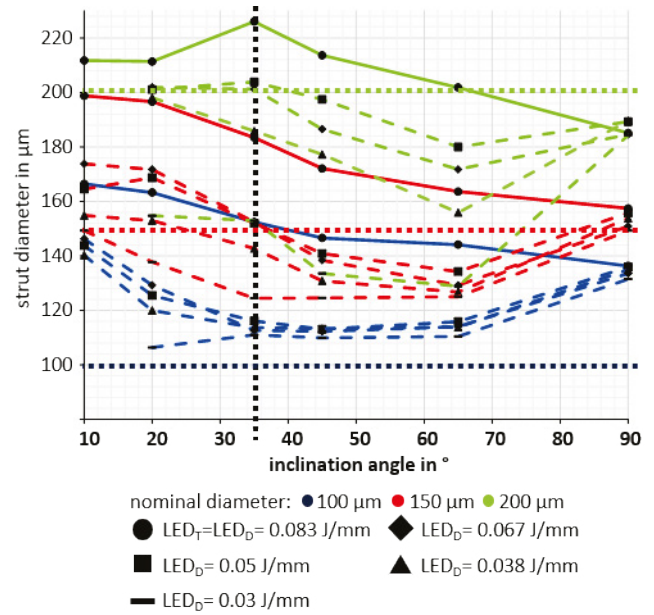


Fig. 9. Influence of  $LED_D$  depending on inclination angle and nominal diameter

quality strut with a diameter of 110 μm at an overhang angle of 35° using an  $LED_D$  value of 0.03 J/mm. However, this parameter set would be unsuitable for diameters > 150 μm, as derived from Fig. 9. Instead, an  $LED_D$  value of 0.05 J/mm showed the lowest deviation across all nominal diameters (intersections of the horizontal and vertical dashed lines). Explaining, why this set was transferred to BCC lattice structures and evaluated in stage three for a scalable and optimized manufacturing accuracy for graded lattice structures. Therefore, depending on the dominant angle of a lattice structure, an  $LED_D$  value should be selected that results in the smallest deviation across all nominal diameters, since a reduced angular dependence is still to be expected despite adaptation.

### 3.3. Applicability for graded and ungraded lattice structures

After choosing  $LED_T = 0.083$  J/mm and  $LED_D = 0.05$  J/mm as most suitable for a BCC diameter scaling, this set was compared to no local adjustment with a constant LED across the contour scan, in regard to the resulting strut diameter and relative density. Fig. 10 (a) summarizes the results for each set comparing the as designed and resulting diameter. While a lower  $LED_T = LED_D$  value of 0.05 J/mm results in nearly no oversizing for 100 μm (15%), an increasing nominal diameter results in an increasing undersizing of down to 14.4% for 300 μm. Conversely, a higher  $LED_T = LED_D$  value of 0.083 J/mm results in a significant oversizing for 100 μm by 38.2%, while an increasing nominal diameter leads to a decreasing oversizing of down to 1.5% for 300 μm. Since it was shown in Fig. 8 and Fig. 9 that particularly small strut diameters are susceptible to a reduced  $LED_D$ , a reduction should have less influence on the nominal diameter of 300 μm and instead improve the accuracy for 100 μm. A splitting into  $LED_T = 0.083$  J/mm and  $LED_D = 0.05$  J/mm increased slightly the deviation for the lower diameter to 19.5%, but drastically improved the accuracy across all nominal diameters with < 1%

for 150  $\mu\text{m}$ , 1.5% for 200  $\mu\text{m}$ , 2.4% for 250  $\mu\text{m}$  and 3% for 300  $\mu\text{m}$ . This means that the established parameter set and adapted strategy can be applied to graded structures without expecting significant over- or undersizing in the respective boundary areas of  $100\ \mu\text{m} < \varnothing < 300\ \mu\text{m}$ .

In contrast, the used set of hatching parameters significantly decreased the relative density with an increasing nominal diameter, as summarized in Fig. 10 (b). While the energy input was sufficient to produce an almost completely dense lattice structure (99.99%) for a nominal diameter of 100  $\mu\text{m}$ , it was

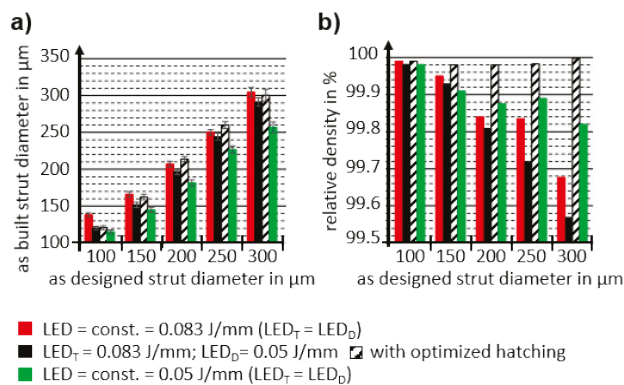


Fig. 10. Comparison of local energy adaptation with constant values on the (a) manufacturing accuracy and (b) relative density for different nominal strut diameters (BCC)

not sufficient enough for larger nominal diameters, reducing the relative density to 99.57–99.82%, with lack of fusion defects mainly occurring in the node sections. This can be explained by Fig. 3 (b) due to the multiple energy input resulting from a spot overlap of nearly 50% for nominal diameters of 100  $\mu\text{m}$  during the contour scan, the local energy input is sufficient enough to achieve high densities, while the relative density of larger nominal diameters depends mostly on optimized hatching parameters. As the energy input at 50 W was not sufficient, despite a recommended VED of 65 J/mm<sup>3</sup>, an optimized parameter set with an increased laser power of 100 W ( $h_d = 80\ \mu\text{m}$ ,  $v = 641\ \text{mm/s}$ ) and equal VED was used and combined with the adapted LED<sub>D</sub>. This improved the relative density across all nominal diameters to 99.98–99.99%, but due to an increased laser power slightly increased the deviation for the respective nominal diameters of 150  $\mu\text{m}$  to 8%, 200  $\mu\text{m}$  to 6.9% and 250  $\mu\text{m}$  to 1%, while achieving nearly 0% deviation for 300  $\mu\text{m}$ . Fine tuning both parameters is therefore necessary to ensure both fully dense lattice structures and a high accuracy manufacturing.

#### 4. Conclusion

This work has demonstrated that local laser power adaptation improves the manufacturing accuracy of BCC lattice structures with nominal diameters in the range of 100–300  $\mu\text{m}$ , applicable for advanced and customized implants including structural grading. The investigations confirm the necessity for advanced process strategies, due to the directional dependency of the process and corresponding geometrical defect of inclined struts. Therefore, the cross-section of the scan path was divided into a top and down section with deviating energy input (LED<sub>T</sub>, LED<sub>D</sub>), which results in a

reduced direction dependency and reduced overmelting. It was also shown that smaller nominal diameters and low inclination angles are more affected due to the larger proportion of exposed powder area. In contrast, larger nominal diameters are more prone to insufficient melting and undersizing if the LED<sub>D</sub> value is too low. Therefore, the optimal parameter set has to be established depending on the dominant inclination angle of the lattice type to counteract this effect. Using the example of a BCC lattice structure (35.26°), the best parameter set (LED<sub>T</sub> = 0.083 J/mm and LED<sub>D</sub> = 0.05 J/mm) reduced the deviation drastically across the evaluated diameter range (19.5% for 100  $\mu\text{m}$ , < 1% for 150  $\mu\text{m}$ , 1.5% for 200  $\mu\text{m}$ , 2.4% for 250  $\mu\text{m}$  and 3% for 300  $\mu\text{m}$ ) without an extensive compromise for either the lower or upper diameter range. With further optimization of the hatch parameters, it was also possible to produce almost fully dense lattice structures (99.99%) for all nominal diameters, highlighting the necessity to fine tune the contour and hatch scanning to ensure both fully dense lattice structures and a high accuracy manufacturing. Future research will focus on introducing dimensionless scaling laws for further optimization and analyzing the local laser adaptation on the resulting mechanical characteristics of graded and new developed designs of lattice structures for advanced implants.

#### Acknowledgements

The authors acknowledge the financial support by the Federal Ministry of Education and Research (BMBF) through Grant Agreement No. 01DQ22002A for the project “add-bite”.

#### References

- [1] Vignesh, M., Ranjith Kumar, G., Sathishkumar, M. *et al.* Development of Biomedical Implants through Additive Manufacturing: A Review. *J. of Materi Eng and Perform* 30, 4735–4744 (2021). <https://doi.org/10.1007/s11665-021-05578-7>
- [2] Martine McGregor, Sagar Patel, Stewart McLachlin, Mihaela Vlasea, Architectural bone parameters and the relationship to titanium lattice design for powder bed fusion additive manufacturing, *Additive Manufacturing*, Volume 47, 2021, 102273, ISSN 2214-8604, <https://doi.org/10.1016/j.addma.2021.102273>.
- [3] Bey Vrancken, Lore Thijs, Jean-Pierre Kruth, Jan Van Humbeeck, Heat treatment of Ti6Al4V produced by Selective Laser Melting: Microstructure and mechanical properties, *Journal of Alloys and Compounds*, Volume 541, 2012, Pages 177–185, ISSN 0925-8388, <https://doi.org/10.1016/j.jallcom.2012.07.022>.
- [4] M. Niinomi, M. Nakai, “Titanium-Based Biomaterials for Preventing Stress Shielding between Implant Devices and Bone”, *International Journal of Biomaterials*, vol. 2011, Article ID 836587, 10 pages, 2011. <https://doi.org/10.1155/2011/836587>
- [5] Enrique Alabort, Daniel Barba, Roger C. Reed, Design of metallic bone by additive manufacturing, *Scripta Materialia*, Volume 164, 2019, Pages 110–114, ISSN 1359-6462, <https://doi.org/10.1016/j.scriptamat.2019.01.022>.
- [6] Xingchen Yan, Qing Li, Shuo Yin, Ziyu Chen, Richard Jenkins, Chaoyue Chen, Jiang Wang, Wenyou Ma, Rodolphe Bolot, Rocco Lupoi, Zhongming Ren, Hanlin Liao, Min Liu, Mechanical and in vitro study of an isotropic Ti6Al4V lattice structure fabricated using selective laser melting, *Journal of Alloys and Compounds*, Volume 782, 2019, Pages 209–223, ISSN 0925-8388, <https://doi.org/10.1016/j.jallcom.2018.12.220>.
- [7] Naoya Taniguchi, Shunsuke Fujibayashi, Mitsuru Takemoto, Kiyoyuki Sasaki, Bungo Otsuki, Takashi Nakamura, Tomiharu Matsushita, Tadashi Kokubo, Shuichi Matsuda, Effect of pore size on bone ingrowth into porous titanium implants fabricated by additive manufacturing: An in vivo experiment, *Materials Science and Engineering: C*, Volume 59, 2016,

- Pages 690-701, ISSN 0928-4931, <https://doi.org/10.1016/j.msec.2015.10.069>.
- [8] I. Maskery, A.O. Aremu, L. Parry, R.D. Wildman, C.J. Tuck, I.A. Ashcroft, Effective design and simulation of surface-based lattice structures featuring volume fraction and cell type grading, *Materials & Design*, Volume 155, 2018, Pages 220-232, ISSN 0264-1275, <https://doi.org/10.1016/j.matdes.2018.05.058>.
- [9] Long Bai, Yue Xu, Xiaohong Chen, Liming Xin, Junfang Zhang, Kun Li, Yuanxi Sun, Improved mechanical properties and energy absorption of Ti6Al4V laser powder bed fusion lattice structures using curving lattice struts, *Materials & Design*, Volume 211, 2021, 110140, ISSN 0264-1275, <https://doi.org/10.1016/j.matdes.2021.110140>.
- [10] C. Qiu, S. Yue, N.J.E. Adkins, M. Ward, H. Hassanin, P.D. Lee, P.J. Withers, M.M. Attallah, Influence of processing conditions on strut structure and compressive properties of cellular lattice structures fabricated by selective laser melting, *Mater. Sci. Eng. A* 628 (2015) 188–197.
- [11] Cao, X., Carter, L.N., Villap  n, V.M., Cantaboni, F., De Sio, G., Lowther, M., Louth, S.E.T., Grover, L., Ginestra, P. and Cox, S.C. (2022), "Optimisation of single contour strategy in selective laser melting of Ti-6Al-4V lattices", *Rapid Prototyping Journal*, Vol. 28 No. 5, pp. 907-915. <https://doi.org/10.1108/RPJ-04-2021-0103>
- [12] Tsopanos, S., Mines, R. A. W., McKown, S., Shen, Y., Cantwell, W. J., Brooks, W., and Sutcliffe, C. J. (July 23, 2010). "The Influence of Processing Parameters on the Mechanical Properties of Selectively Laser Melted Stainless Steel Microlattice Structures." *ASME. J. Manuf. Sci. Eng.* August 2010; 132(4): 041011. <https://doi.org/10.1115/1.4001743>
- [13] Hanemann, T. (2022). Usability and limitations of dimensionless scaling laws in Laser Powder Bed Fusion
- [14] Shaaz Ghouse, Sarat Babu, Richard J. Van Arkel, Kenneth Nai, Paul A. Hooper, Jonathan R.T. Jeffers, The influence of laser parameters and scanning strategies on the mechanical properties of a stochastic porous material, *Materials & Design*, Volume 131, 2017, Pages 498-508, ISSN 0264-1275, <https://doi.org/10.1016/j.matdes.2017.06.041>.
- [15] Alexander M. Rubenchik, Wayne E. King, Sheldon S. Wu, Scaling laws for the additive manufacturing, *Journal of Materials Processing Technology*, Volume 257, 2018, Pages 234-243, ISSN 0924-0136, <https://doi.org/10.1016/j.jmatprotec.2018.02.034>.
- [16] Lu Liu, Paul Kamm, Francisco Garc  a-Moreno, John Banhart, Damiano Pasini, Elastic and failure response of imperfect three-dimensional metallic lattices: the role of geometric defects induced by Selective Laser Melting, *Journal of the Mechanics and Physics of Solids*, Volume 107, 2017, Pages 160-184, ISSN 0022-5096, <https://doi.org/10.1016/j.jmps.2017.07.003>.
- [17] Y. Solyaev, L. Rabinskiy, D. Tokmakov, Overmelting and closing of thin horizontal channels in AlSi10Mg samples obtained by selective laser melting, *Additive Manufacturing*, Volume 30, 2019, 100847, ISSN 2214-8604, <https://doi.org/10.1016/j.addma.2019.100847>.
- [18] Umar Hossain, Shaaz Ghouse, Kenneth Nai, Jonathan R.T. Jeffers, Mechanical and morphological properties of additively manufactured SS316L and Ti6Al4V micro-struts as a function of build angle, *Additive Manufacturing*, Volume 46, 2021, 102050, ISSN 2214-8604, <https://doi.org/10.1016/j.addma.2021.102050>.
- [19] Wang, D., Yang, Y., Yi, Z. et al. Research on the fabricating quality optimization of the overhanging surface in SLM process. *Int J Adv Manuf Technol* 65, 1471–1484(2013) <https://doi.org/10.1007/s00170-012-4271-4>
- [20] H.M. Khan, M.H. Dirikolu, E. Ko  , Parameters optimization for horizontally built circular profiles: Numerical and experimental investigation, *Optik*, Volume 174, 2018, Pages 521-529, ISSN 0030-4026, <https://doi.org/10.1016/j.ijleo.2018.08.095>.
- [21] Leonhard Hitzler, Christoph Janousch, Jochen Schanz, Markus Merkel, Burkhard Heine, Florian Mack, Wayne Hall, Andreas   chsner, Direction and location dependency of selective laser melted AlSi10Mg specimens, *Journal of Materials Processing Technology*, Volume 243, 2017, Pages 48-61, ISSN 0924-0136, <https://doi.org/10.1016/j.jmatprotec.2016.11.029>.
- [22] Zhichao Dong, Yabo Liu, Weijie Li, Jun Liang, Orientation dependency for microstructure, geometric accuracy and mechanical properties of selective laser melting AlSi10Mg lattices, *Journal of Alloys and Compounds*, Volume 791, 2019, Pages 490-500, ISSN 0925-8388, <https://doi.org/10.1016/j.jallcom.2019.03.344>.
- [23] Zahra S. Bagheri, David Melancon, Lu Liu, R. Burnett Johnston, Damiano Pasini, Compensation strategy to reduce geometry and mechanics mismatches in porous biomaterials built with Selective Laser Melting, *Journal of the Mechanical Behavior of Biomedical Materials*, Volume 70, 2017, Pages 17-27, ISSN 1751-6161, <https://doi.org/10.1016/j.jmbbm.2016.04.041>.
- [24] Radek Vr  na, Jan Jaro  , Daniel Koutn  y, Jakub Nosek, Tom    Zikmund, Jozef Kaiser, David Palou  ek, Contour laser strategy and its benefits for lattice structure manufacturing by selective laser melting technology, *Journal of Manufacturing Processes*, Volume 74, 2022, Pages 640-657, ISSN 1526-6125, <https://doi.org/10.1016/j.jmapro.2021.12.006>.
- [25] Horn, M., Koch, L., Schafnitzel, M., Schmitt, M., Schlick, G., Schilp, J. & Reinhart, G. (2021). Parametric compensation scheme for increasing the geometrical accuracy of lattice structures in medical implants produced by powder bed fusion. *Procedia CIRP*, 104, 839–844. <https://doi.org/10.1016/j.procir.2021.11.141>
- [26] Gaur, B., Soman, D., Ghysar, R. and Bhallamudi, R. (2023), "Ti6Al4V scaffolds fabricated by laser powder bed fusion with hybrid volumetric energy density", *Rapid Prototyping Journal*, Vol. 29 No. 1, pp. 67-79. <https://doi.org/10.1108/RPJ-01-2022-0036> [Titel anhand dieser DOI in Citavi-Projekt   bernehmen]
- [27] Ulff, N., Schubert, J., & Zanger, F. (2023, November). Potential of Scanning-Strategy Adaptations for Producing Homogenous Microlattices by PBF-LB. In *Congress of the German Academic Association for Production Technology* (pp. 747-756). Cham: Springer Nature Switzerland
- [28] Buhairi, M.A., Foudzi, F.M., Jamhari, F.I. et al. Review on volumetric energy density: influence on morphology and mechanical properties of Ti6Al4V manufactured via laser powder bed fusion. *Prog Addit Manuf* 8, 265–283 (2023). <https://doi.org/10.1007/s40964-022-00328-0>
- [29] Shuai Chang, Aihong Liu, Chun Yee Aaron Ong, Lei Zhang, Xiaolei Huang, Yong Hao Tan, Liping Zhao, Liqun Li & Jun Ding (2019) Highly effective smoothening of 3D-printed metal structures via overpotential electrochemical polishing, *Materials Research Letters*, 7:7, 282-289, DOI: 10.1080/21663831.2019.1601645